



This is a repository copy of *One-Step Synthesis of Graphene Oxide-Polyamidoamine Dendrimer Nanocomposite Hydrogels by Self-Assembly*.

White Rose Research Online URL for this paper:

<http://eprints.whiterose.ac.uk/102189/>

Version: Accepted Version

Article:

Piao, Y., Wu, T. and Chen, B. (2016) One-Step Synthesis of Graphene Oxide-Polyamidoamine Dendrimer Nanocomposite Hydrogels by Self-Assembly. *Industrial and Engineering Chemistry Research*, 55 (21). pp. 6113-6121. ISSN 0888-5885

<https://doi.org/10.1021/acs.iecr.6b00947>

Reuse

Unless indicated otherwise, fulltext items are protected by copyright with all rights reserved. The copyright exception in section 29 of the Copyright, Designs and Patents Act 1988 allows the making of a single copy solely for the purpose of non-commercial research or private study within the limits of fair dealing. The publisher or other rights-holder may allow further reproduction and re-use of this version - refer to the White Rose Research Online record for this item. Where records identify the publisher as the copyright holder, users can verify any specific terms of use on the publisher's website.

Takedown

If you consider content in White Rose Research Online to be in breach of UK law, please notify us by emailing eprints@whiterose.ac.uk including the URL of the record and the reason for the withdrawal request.

One-step synthesis of graphene oxide-polyamidoamine dendrimer nanocomposite hydrogels by self-assembly

*Yongzhe Piao, Tongfei Wu and Biqiong Chen**

Department of Materials Science and Engineering, University of Sheffield, Mappin Street,
Sheffield S1 3JD, UK

ABSTRACT: Graphene oxide (GO)-polyamidoamine (PAMAM) dendrimer nanocomposite hydrogels were prepared through one-step synthesis by mixing a GO suspension and a PAMAM solution at varying ratio of GO to PAMAM. The materials self-assembled into physically cross-linked networks, mainly driven by electrostatic interactions between the oppositely charged GO nanosheets and PAMAM dendrimer. The chemical structure of PAMAM dendrimer was studied by mass spectrometry, nuclear magnetic resonance spectroscopy and potentiometric titration. The structure and properties of GO-PAMAM nanocomposite hydrogels were investigated by Fourier transform infrared spectroscopy, Raman spectroscopy, X-ray diffraction, scanning electron microscopy and rheometry. The nanocomposite hydrogels exhibited a relatively high mechanical performance with a storage modulus of up to 284 kPa, as well as self-healing property, owing to their reversible and multiple physical cross-links. These hydrogels may be further developed for biomedical applications.

1. INTRODUCTION

Hydrogels are attractive for the biomedical field due to their excellent biocompatibility and biomimetic microenvironment.^{1,2} However, conventional hydrogels are commonly fragile and involve toxic organic cross-linkers in their synthesis, limiting their applications.

Graphene oxide (GO) is a two-dimensional nanomaterial, having a high specific surface area, high fracture strength and high modulus as well as good hydrophilicity.³ The plentiful amount of oxygen-containing functional groups on GO sheets provide easy modification of GO for various applications.^{4,5} Biopolymer surface-functionalized GO nanosheets were reported to be biocompatible and non-toxic at low concentrations.^{6,7} GO has recently been applied to prepare polymer nanocomposite hydrogels with improved mechanical performance compared to conventional hydrogels,^{8,9} and various self-assembly approaches were used to prepare physically cross-linked GO-polymer nanocomposite hydrogels.^{10,11} The driving forces to form these hydrogels were physical interactions including π - π interaction, hydrogen bonding, electrostatic interaction and coordination.¹² Shi's group synthesized a supramolecular GO-poly(vinyl alcohol) hydrogel, containing 99.2 wt% water, by self assembly, showing a storage modulus of 0.2 kPa.¹⁰ They also self-assembled a GO-DNA hydrogel with a similar amount of water by a hydrothermal method, which showed a storage modulus of about 4.6 kPa.¹¹ Hydrogels self-assembled by mixing GO and cationic polymers in water were later also reported by others.¹³⁻¹⁵ GO-polyamine hydrogels, including tris(aminoethyl)-amine, spermine, and spermidine, were formed driven by electrostatic interaction (mechanical properties not shown).¹³ GO/branched polyethylenimine (PEI) hydrogels were reported for organic dye removal and wastewater treatment (mechanical properties not shown).¹⁶ We reported that GO-gelatin nanocomposite hydrogels having 98 wt.% water exhibited a storage modulus of 115 kPa.¹⁴ GO-chitosan hydrogels with 99.4–99.5 wt%

water were reported as broad-spectrum adsorbents for water purification, possessing a storage modulus of 10–400 kPa.¹⁵ A much lower value of 0.7 kPa for a GO-chitosan hydrogel was reported by another group,¹⁷ despite of a lower water content (91.7 wt%). This was presumably owing to the different synthesis method utilized for the latter and the lower concentration of GO (0.3 wt%) in the final hydrogel compared to that (0.5 wt%) in the former. While possessing attractive properties such as stimuli-responsiveness^{10,14} and self-healing,¹¹ the above self-assembled hydrogels were generally still weak, limiting them to be applied to broader fields, e.g. load-bearing soft tissue engineering.

Dendrimers are a type of organic molecules which are highly branched and monodisperse.¹⁸ Polyamidoamine (PAMAM) dendrimers have been widely studied in the biomedical field due to their low cytotoxicity, controllable size and easy functionalization.¹⁹ Chemically crosslinked collagen scaffolds with incorporation of amine-terminated PAMAM dendrimer were reported, where the dendrimer was used as an additional cross-linker to improve their mechanical properties.²⁰ A number of PAMAM-poly(ethylene glycol) hydrogels were investigated for versatile biomedical platforms, in which PAMAM was the primary building component.^{21,22} Recently, Wang and co-workers²³ developed mouldable hydrogels with 94.5–97.7 wt% water using clay and a dendritic molecular binder, showing storage moduli of 30–500 kPa. The pronounced mechanical property was ascribed to strong electrostatic interactions between the two building components and the high density of cross-linking sites of dendritic molecules.²³ This implied self-assembly of GO and PAMAM dendrimer could also lead to mechanically strong nanocomposite hydrogels due to the multiple oxygenated functional groups and excellent mechanical properties of GO sheets.

The combination of PAMAM dendrimers and graphene derivatives has been introduced to develop hybrid nanomaterials in different forms. Reduced GO (RGO) nanosheets modified by PAMAM dendrimers were reported for catalysis.^{24,25} RGO-PAMAM-silver nanoparticles were prepared for electrode applications and biosensing.²⁶ PAMAM-modified GO nanosheets and GO-PAMAM composites, showing an excellent adsorption ability, were investigated for removing heavy metal ions from waste water.^{27,28} GO and hyperbranched dimethylolpropionic acid polyester-toughened poly(acrylic acid) hydrogels with high water absorption ability and excellent mechanical properties were also reported.²⁹ PAMAM dendrimers have an advantage over linear chain polymers on hydrogel gelation, because they have much more functional end groups available for cross-linking and so the cross-linking density of the resulting hydrogels are expected to be higher and hence their mechanical performance.³⁰ In addition, the dendrimers could be readily modified to modulate the chemical, physical and biological properties where necessary.²¹ In the current work, physically cross-linked GO-PAMAM nanocomposite hydrogels were prepared through a simple self-assembly approach, and their structure, rheological properties, formation mechanism and self-healing property were investigated.

2. EXPERIMENTAL

2.1 Materials. Graphite powder (particle size < 20 µm), concentrated sulphuric acid (98%), hydrochloric acid (35%), potassium permanganate, sodium nitrate, hydrogen peroxide (30%), ethylenediamine (EDA) (\geq 99.5%), methanol (\geq 99.9%), methylacrylate (MA) (99%) and deuterium oxide (D₂O) (99.9 atom% D) were all obtained from Sigma-Aldrich Corporation.

2.2 Preparation of PAMAM dendrimer G4.0. The PAMAM dendrimer Generation 4.0 (G4.0) was prepared following a method described in the previous literature.³¹ Briefly, an EDA

methanol solution was prepared and cooled down to -20 °C using an ice bath, to which methanolic MA was added drop-wise under agitation. The resultant solution was reacted at 25 °C for 2 days and at 40 °C for 4 days. The excess MA and solvent were removed by vacuum distillation below 40 °C, leading to a half-generation dendrimer (multi-ester).³² Then the multi-ester methanol solution was prepared and cooled down to -20 °C. The solution was slowly added to the pre-cooled EDA methanol solution, which was kept below -10 °C. The resulting solution was allowed to react at 25 °C for 2 days and at 40 °C for 4 days, followed by removal of the excess EDA and solvent. As a result, a pale amber-coloured syrup, a full-generation dendrimer,³² was obtained. This whole process was further replicated four times to achieve the PAMAM dendrimer G4.0 for subsequent studies.

2.3. Preparation of GO-PAMAM nanocomposite hydrogels. GO was prepared using graphite following a modified Hummers' method,^{33,34} and purified and freeze-dried.¹⁴ GO-PAMAM nanocomposite hydrogels were synthesized by one-step self assembly. Typically, a PAMAM water solution (0.5 mL) with a desired concentration was added drop by drop into a GO suspension (5.5 mL) under stirring to form a hydrogel in about 30 seconds. Two sets of hydrogels were prepared. In one set, the GO concentration in the hydrogel was 10 mg mL⁻¹, and the PAMAM concentration varied as 0.5, 1, 5, 10, 20 and 30 mg mL⁻¹. In the other set, PAMAM was kept at 10 mg mL⁻¹, while GO varied as 6, 8 and 10 mg mL⁻¹. The hydrogel products were denoted as GmDnH, in which m and n defined the concentrations of GO and PAMAM, respectively.

2.4 Characterization. The dendrimer (5 mg mL⁻¹) was dissolved in D₂O and analysed on a Bruker DRX-500 (500 MHz) nuclear magnetic resonance spectroscopy (NMR) at 25 °C for ¹H with the solvent proton signal as an internal reference. The spectrometer was equipped with an

inverse geometry 5 mm VSP probe with a single z-gradient. The operation software version was TOPSPIN 1.3. The mass spectrum of the PAMAM dendrimer was obtained on a Bruker Reflex III MALDI-TOF mass spectrometer. The matrix solution was sinapic acid (10 mg mL^{-1}) in acetonitrile: water: trifluoroacetic acid (weight ratio, 50: 50: 0.1). The concentration of PAMAM dendrimer in the matrix solution was 1 mg mL^{-1} . Before testing, the mass spectrometer was calibrated with the matrix solution containing known peptides. Titrations were performed on a Multiparameter (SevenExcellenceTM) and an INLAB Expert Pro-ISM pH electrode (Mettler Toledo) at ambient temperature ($23 \pm 1^\circ\text{C}$) in nitrogen environment. PAMAM dendrimer (13 mg) was dissolved in a 10 mL 0.1 M NaCl solution. 0.1001 M HCl and 0.0999 M NaOH were used for forward and back titrations, respectively. GO (40 mg) was dispersed in 10 mL 0.1 M NaCl solution by 30 min sonication before the suspension was tuned using the standard NaOH solution to pH = 10, and then titrated by the standard HCl solution to pH = 2.30. The titrant was added by 0.03 mL portions using a pipette (Eppendorf Research Plus, Eppendorf, Germany). Laser scattering particle sizing was performed on a Coulter LS130 (ranging from 0.1 to 900 μm) by 3 runs with graphite powder and fully exfoliated GO nanosheets in an aqueous suspension (0.5 mg mL^{-1}) respectively.

Fourier transform infrared spectroscopy (FT-IR) was conducted on an IR Spectrometer (Spectrum 100, Perkin Elmer) with a resolution of 4 cm^{-1} . Raman spectra were recorded on a Raman Spectroscope (Renishaw inVia) equipped with a laser with an excitation wavelength (λ) of 514.5 nm and operated at 1.0 mW. Samples were placed onto a clear glass plate. The spectra were acquired by accumulating three acquisitions of 10 seconds with a 50 \times objective. X-ray diffraction (XRD) curves were obtained on an X-ray diffractometer (STOE STADI P) with Cu K α_1 radiation ($\lambda = 0.15406 \text{ nm}$) at 35 mA and 40 kV. The scan speed was $0.27^\circ \text{ s}^{-1}$ and the step

size was 0.03° (2θ). Scanning electron microscopy (SEM) was achieved with an Inspect F SEM (FEI) at an accelerating voltage of 10 kV. Freeze-dried samples were used for these structural and morphological analyses; the hydrogels were pre-frozen at -30°C for 24 h, and then lyophilized at -10°C for 48 h in a FreeZone Triad Freeze Dry System (Labco Corporation). Before SEM analysis, the fracture surfaces of the freeze-dried GO and GO-PAMAM nanocomposite hydrogels were coated with gold using an Emscope SC500A sputter coater. The pore sizes were averaged from at least 40 pores using ImageJ software. Rheological tests were performed on an MCR 301 rheometer (Anton Paar) using 25 mm parallel plates. The sweep range of angular frequency was between 0.1 and 100 rad s^{-1} . The strain was set at 0.1% within the linear viscoelastic zone, while the test gap was fixed at 2.0 mm.

3. RESULTS AND DISCUSSION

3.1 Characterization of PAMAM dendrimer G4.0. Synthesis of the PAMAM dendrimer was a two-step process, using an initiator core, EDA. After a continuous process, the PAMAM dendrimer with $-\text{NH}_2$ terminal groups was obtained. The chemical shifts in the ^1H NMR spectrum (500 MHz, D_2O) of the prepared PAMAM dendrimer (Fig.1) appear at $\delta = 2.36$ (H_c), 2.55 (H_a and H_e), 2.66 (H_g), 2.75 (H_b), 3.18 (H_f) and 3.22 ppm (H_d), which can be identified with the protons assigned with the same letters in the theoretical PAMAM dendrimer fragment. These chemical shifts are consistent with the results reported in the previous papers,^{35,36} initially verifying the molecular structure and confirming the successful synthesis of the PAMAM dendrimer G4.0.

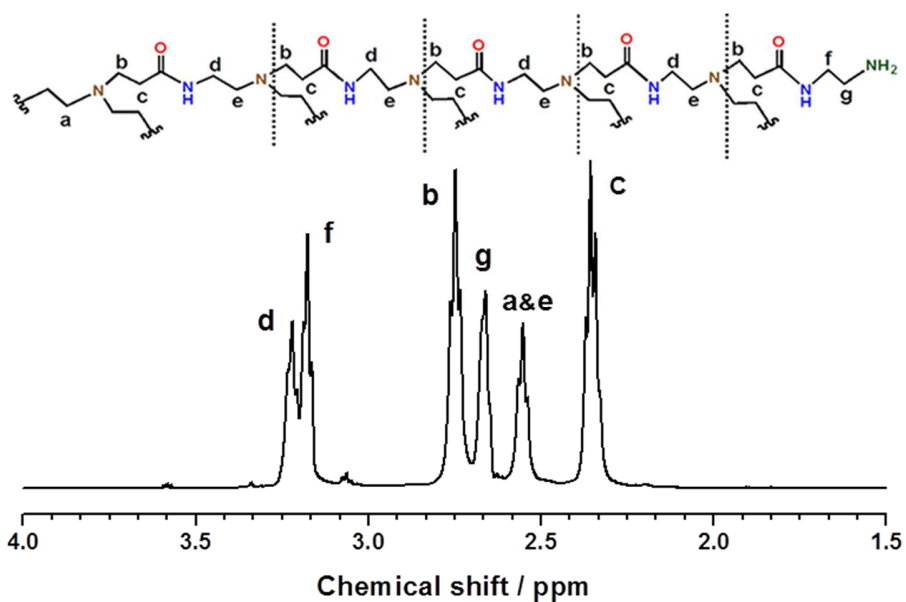


Figure 1. ^1H NMR spectrum of the PAMAM dendrimer G4.0 and peak assignments corresponding to the protons denoted in the fragment of a PAMAM dendrimer.

The molecular weight of the PAMAM dendrimer G4.0 prepared, determined by mass spectrometry (MS), is 9,534 Dalton (Fig. 2(A)), which is lower than the theoretical value of 14,196 for PAMAM dendrimer G4.0 with an ideal structure.³¹ The deviation of the resultant molecular weight from the original synthesis design was presumably due to incomplete Michael addition, intramolecular cyclization, and fragmentation arising from the retro-Michael reaction.³¹ This deviation could also be partially attributed to the measurement system as reported in the literature.³⁷

Curve a in Fig. 2(B) shows that the PAMAM dendrimer is basic ($\text{pH} = 9.26$) in an aqueous solution (1.3 mg mL^{-1}) before titration. The turning points during the back titration (curve b) show the distinctive start and end points of protonation, which is consistent with the previous report³¹ for PAMAM dendrimers. According to the first derivative peaks, the start and end points of deprotonation are at $\text{pH} = 4.05$ and $\text{pH} = 7.51$ for tertiary amines and at $\text{pH} = 7.51$ and $\text{pH} = 10.51$ for primary amines, respectively. Because the geometric structure of the PAMAM

dendrimer G4.0 is globular, only the peripheral primary amine ($-NH_2$) groups can participate in electrostatic attractions with GO sheets. The number of $-NH_2$ groups present in the dendrimer can be calculated according to the consumption of OH^- ions during deprotonation of $-NH_2$ groups and the molecular weight estimated from MS.³⁸ Considering the minimum volumetric addition (0.03 mL) during the titration, the number of $-NH_2$ groups in our PAMAM dendrimer is 46 ± 2 . This number is lower than the theoretical value (64) of PAMAM dendrimer G4.0, because of the defects and incomplete reactions as described earlier.³¹

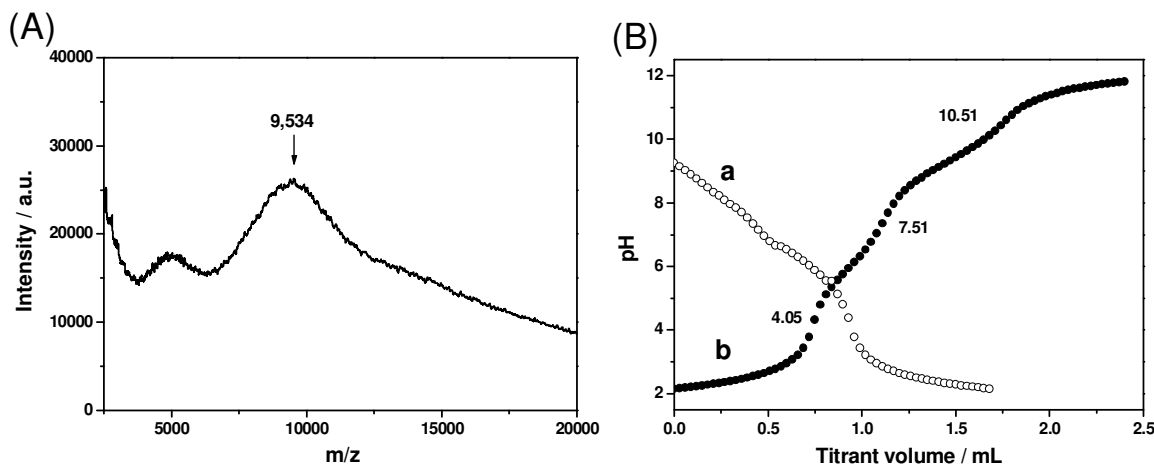


Figure 2. (A) MALDI-TOF mass spectrum of PAMAM dendrimer G4.0. (B) Potentiometric acid-base titration of PAMAM. The forward titration (curve a) and the back titration (curve b) were performed using a 0.1001 M HCl solution and a 0.0999 M NaOH solution, respectively.

3.2 Characterization of GO. The GO nanosheets used to synthesize the nanocomposite hydrogels have been measured by atomic force microscopy (AFM) and thermogravimetric analysis (TGA) in our previous work.¹⁴ The single GO nanosheets have a thickness of 1.0 nm and a typical length of one to several microns¹⁴ (with a new AFM image shown in the inset of Fig. 3(A)). The content of the oxygenated groups in GO was approximately 55 wt% according to TGA analysis.¹⁴ As shown in Fig. 3(A), the raw material, graphite powder, was measured to be between 1.8 and 50 μm in particle size. The majority of the GO nanosheets range in size from

2.2 to 20 μm with a mean of 5.5 μm . This laser sizing measurement records the hydrodynamic diameter of particles by assuming these particles are spherical in shape. The result of GO titration is shown in Fig. 3(B). The titrant (HCl) consumption is mainly attributed to the protonation of carboxyl groups and hydroxyl groups.³⁹ The start point of protonation (at pH = 8.24) is attributed to hydroxyl groups while the end point (at pH = 4.76) is due to more acidic carboxyl groups. However, there is no clear transition point between the two steps, probably because of the surface heterogeneity of GO.^{39,40} This result indicates that the GO suspension is negatively charged above pH = 4.76.

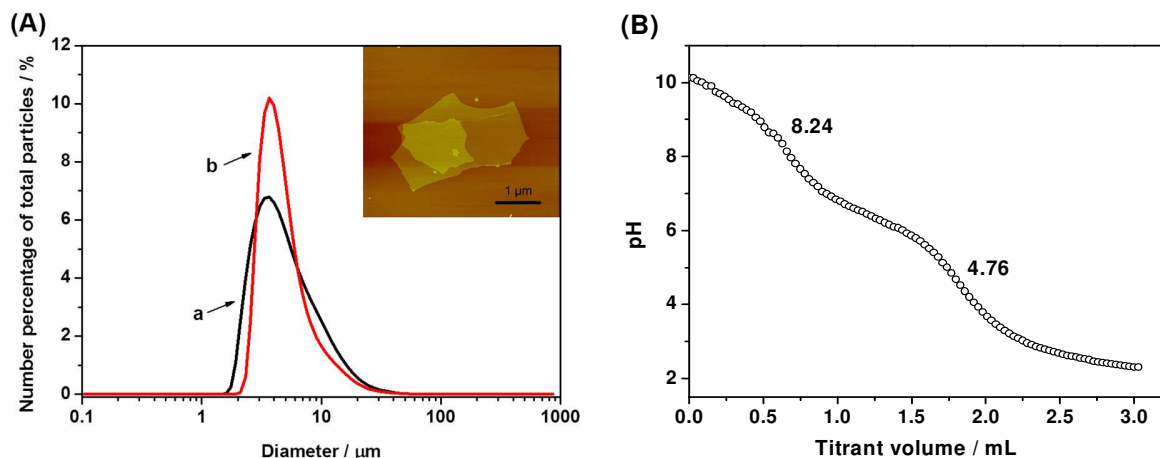


Figure 3. (A) Laser scattering particle sizing profiles of (a) graphite powder and (b) GO nanosheets in an aqueous solution, with an inset of the tapping mode AFM topographic image of two layers of GO; (B) Acid-base titration of GO using a 0.1001 M HCl solution.

3.3 Characterization of GO-PAMAM nanocomposite hydrogels. The GO-PAMAM nanocomposite hydrogels with a fixed concentration of GO were prepared by adding a small portion of a PAMAM solution into an aqueous GO suspension under stirring. Stable hydrogels, G10D1H, G10D5H, G10D10H and G10D20H, were formed and confirmed by the tube inversion test⁴¹ (Fig. S1). Incorporation of less PAMAM dendrimer, G10D0.5H, failed to form a hydrogel,

but a sol (Fig. S1). FT-IR spectra of graphite,¹⁴ GO,¹⁴ neat PAMAM and lyophilized GO-PAMAM nanocomposite hydrogels are presented in Fig. 4(A). Graphite (curve a) only possesses a weak peak at 3400 cm⁻¹ from O–H stretching of residual water.¹⁴ GO (curve b) shows the absorption peaks of C=O (1731 cm⁻¹), C=C (1619 cm⁻¹), C–O–C (1276 cm⁻¹) and C–O (1050 cm⁻¹), as well as O–H (3200–3400 cm⁻¹).^{14,42} The spectrum g has typical characteristics of PAMAM: the vibration peaks for C=O stretching (1631 cm⁻¹), C(O)NH (1545 cm⁻¹), C–H stretching (2933 cm⁻¹), as well as N–H stretching of primary amine (3263 cm⁻¹) and anti-symmetric substituted primary amine (3071 cm⁻¹).⁴³ This further confirms that the PAMAM dendrimer was successfully synthesized. After incorporation of PAMAM, the C=O peak of GO (1731 cm⁻¹) diminishes, and vanishes completely in G10D20H (curve f) and G10D30H (curve g) containing 67 wt% and 75 wt% PAMAM, respectively. This may be explained by the transformation of carboxyl groups of GO to carboxylate complex with the amino groups of PAMAM.^{44,45} Emergence of the C(O)NH bending at 1545 cm⁻¹ and C=O amide I vibration at 1631 cm⁻¹ in curves b-e for the nanocomposites also confirms the incorporation of PAMAM into the hydrogels.

Fig. 4(B) illustrates Raman spectra of the samples. The intense G band at 1580 cm⁻¹ in the spectrum of graphite (curve a) is ascribed to in-phase vibration of the E_{2g} mode of graphite lattice, while a small D band at 1353 cm⁻¹ is contributed to the A_{1g} mode.^{14,46} After oxidation and exfoliation, both bands turn broader (curve b). The intensity ratio (I_D/I_G) increases significantly from 0.08 for graphite to 0.79 in GO, implying a much higher degree of lattice disorder and defects in the latter.^{14,47} Furthermore, the G band of graphite moves to 1598 cm⁻¹, and a new D' band at 1620 cm⁻¹ appears in GO, because of the isolation of double bonds from higher-energy functional groups in GO sheets.^{14,47} GO-PAMAM nanocomposite hydrogels possess similar

spectra (curves c-g) to GO. With an increasing PAMAM content, the G band gradually shifts from 1598 cm^{-1} in GO to 1587 cm^{-1} in G10D30H, attributable to the charge transfer from PAMAM to GO sheets.^{11,14} These results indicate the electrostatic attractions between GO and PAMAM.

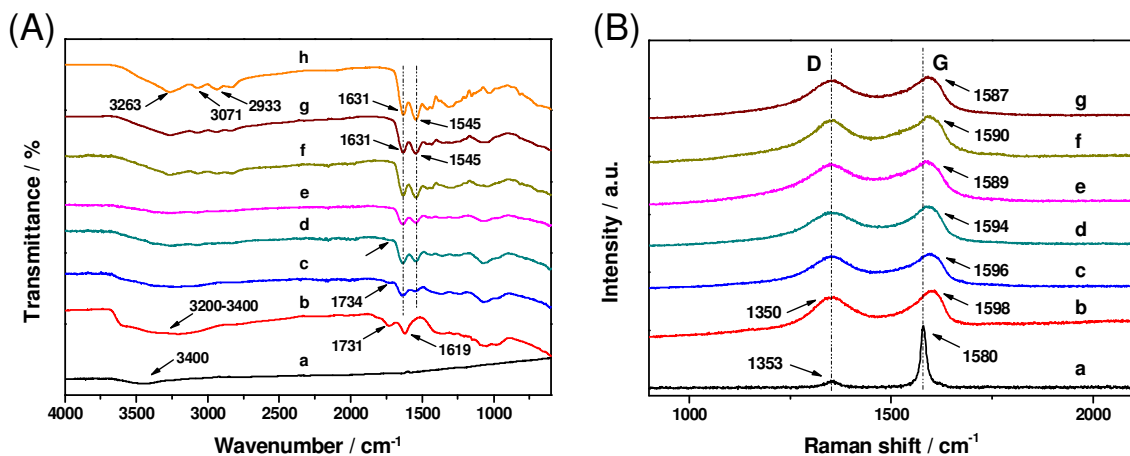


Figure 4. (A) FT-IR and (B) Raman spectra of (a) graphite,¹⁴ (b) lyophilized GO¹⁴ and GO-PAMAM nanocomposite hydrogels: (c) G10D1H, (d) G10D5H, (e) G10D10H, (f) G10D20H, (g) G10D30H, and (h) neat PAMAM dendrimer.

Fig. 5 depicts XRD traces of the samples. Graphite shows a sharp peak at 26.4° corresponding to an interlayer distance (d_{002}) of 0.34 nm .¹⁴ After oxidation, a typical diffraction peak of graphite oxide is observed at 10.6° corresponding to a d_{002} of 0.83 nm , ascribed to the formation of oxygenated groups on graphene.^{14,48} However, the GO diffraction peak disappears in the XRD traces of lyophilized GO-PAMAM nanocomposite hydrogels, indicating an excellent dispersion and exfoliation of GO in the nanocomposites, noting the high contents of GO in the nanocomposites.^{14,49}

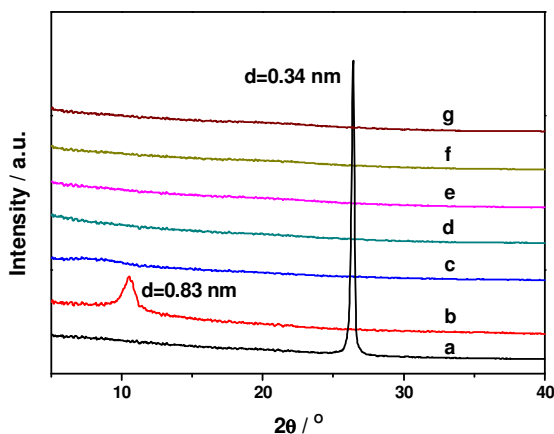


Figure 5. XRD traces of (a) graphite,¹⁴ (b) lyophilized GO,¹⁴ and lyophilized GO-PAMAM nanocomposite hydrogels: (c) G10D1H, (d) G10D5H, (e) G10D10H, (f) G10D20H, and (g) G10D30H.

The interior morphologies of the lyophilized samples were investigated by SEM, as shown in Fig. 6. The nanocomposite hydrogels possess interconnected open porous microstructures which vary with the PAMAM content. The morphology of the nanocomposite with the least PAMAM (G10D1H in Fig. 6(B), average pore size: $6.1 \pm 2.5 \mu\text{m}$) has the least change compared to the structure of the lyophilized GO suspension (Fig. 6(A)). In contrast, more changes occur to G10D5H and G10D10H which exhibit much smaller pore sizes ($2.4 \pm 1.2 \mu\text{m}$ and $2.0 \pm 0.9 \mu\text{m}$, respectively). At higher PAMAM contents, G10D20H (pore size: $3.4 \pm 1.6 \mu\text{m}$) and G10D30H (pore size: $4.9 \pm 2.2 \mu\text{m}$) show significantly different morphological profiles, with more integral and less porous structures. G10D30H possesses less uniform porous structure than G10D20H, presumably due to the higher dendrimer content. Excess dendrimer may cause inhomogeneous cross-linking between GO and PAMAM in the hydrogel, leaving some regions with more solid contents than others. The porous structure of the hydrogel plays an important role in influencing its mechanical properties, which is discussed further subsequently.

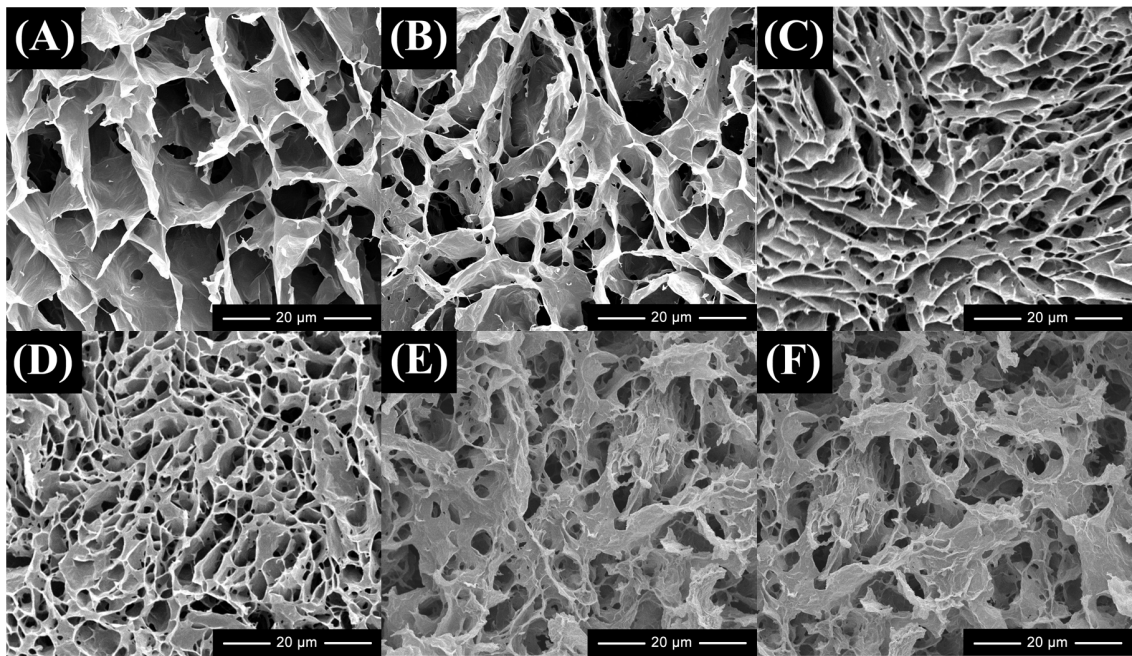
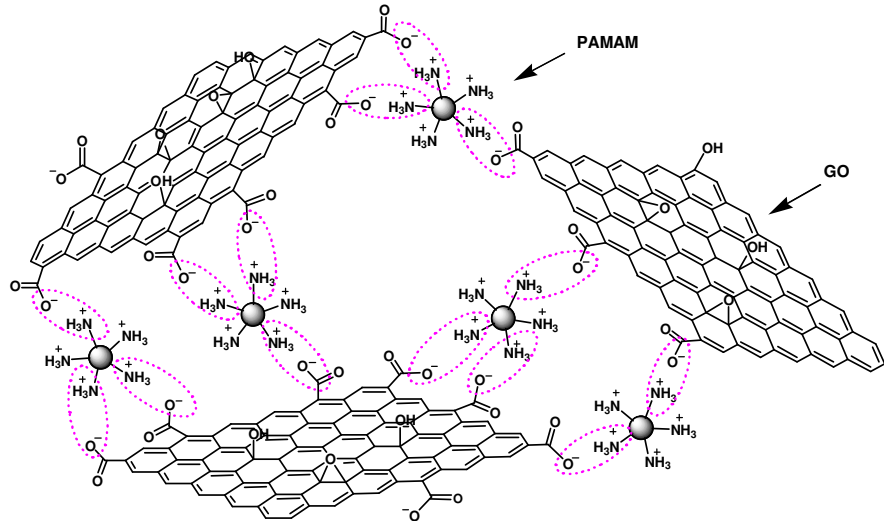


Figure 6. SEM images of lyophilized (A) GO suspension and GO-PAMAM nanocomposite hydrogels: (B) G10D1H, (C) G10D5H, (D) G10D10H, (E) G10D20H, and (F) G10D30H.

The hydrogel network is assembled by physically cross-linking positively charged PAMAM dendrimer (mainly $-NH_2$ groups) and negatively charged GO nanosheets (mainly carboxyl groups). Based on the consumption of the acid or the base by GO or PAMAM during their back titrations (as shown in Fig. 3(B) and Fig. 2(B)), the ratio of the charge moles per unit weight between GO and PAMAM, is calculated to be 0.6. The $-NH_2$ groups at the edge of globular PAMAM becomes protonated by $-COOH$ groups from GO, leading to strong electrostatic attractions between the two materials and the formation of a robust hydrogel (Scheme 1). The charge capacity ratios of GO to PAMAM in the hydrogels are 6/1, 6/5, 6/10, 6/20 and 6/30 for G10D1H, G10D5H, G10D10H, G10D20H and G10D30H, respectively. Since G10D0.5H cannot form a hydrogel, 6/1 is considered as the approximate critical gelation ratio for this system. As expected for many physically cross-linked hydrogels these GO-PAMAM nanocomposite

hydrogels demonstrated self-healing capability, and the self-healing process was relatively fast (Fig. S2) due to the multiple physical crosslinks, e.g., electrostatic interactions.⁵⁰



Scheme 1. Illustration of 3D-network GO-PAMAM nanocomposite hydrogel formed mainly by the electrostatic attractions between the deprotonated carboxyl groups of GO and protonated amino groups of PAMAM.

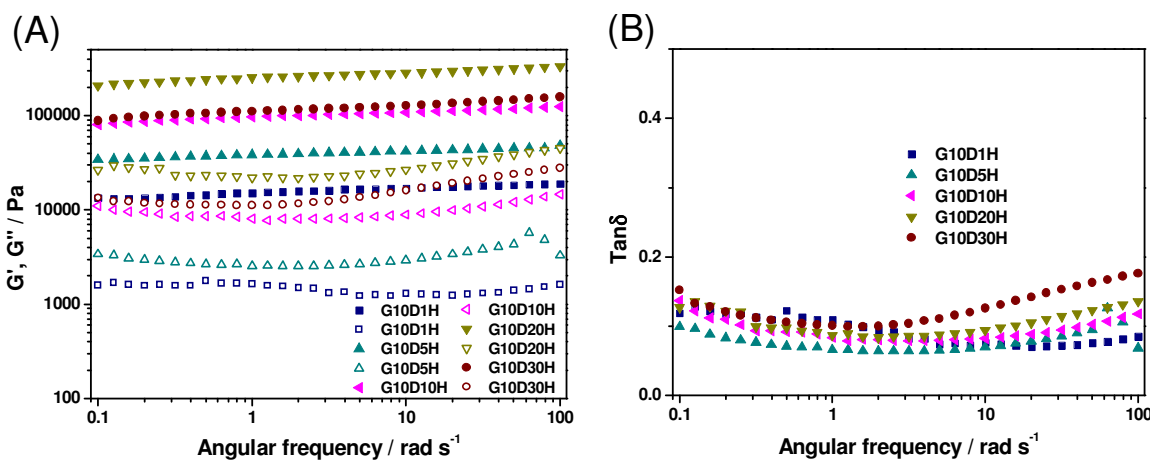
Rheological measurements (Fig. 7) show that storage moduli (G') and loss moduli (G'') of GO-PAMAM nanocomposite hydrogels are nearly independent of angular frequency between 0.1 and 100 rad s⁻¹, confirming the highly elastic characteristic of the hydrogels.¹¹ Furthermore, G' is about one order higher than G'' and the damping factors ($\tan\delta$) are almost independent of frequency, suggesting the formation of stable hydrogels (Fig. 7(B) and 7(D)).⁵¹ Comprising the least PAMAM concentration of 1 mg mL⁻¹, G10D1H has a storage modulus of 17 kPa at 10 rad s⁻¹. The storage modulus of G10D5H, 42 kPa, is 147% higher than that of G10D1H. A more than 5-fold increase is seen in the storage modulus of G10D10H (108 kPa) compared with that of G10D1H, and more significantly, an about 16-fold increase is found for G10D20H with a storage modulus of 284 kPa. This signifies that up to a certain concentration of PAMAM (20 mg mL⁻¹) the hydrogel becomes more elastic with increasing PAMAM content; a higher fraction of

PAMAM results in more effective cross linkages which significantly improves the elasticity of the three-dimensional network. However, a further increase of PAMAM content sees a decrease in the storage modulus to 128 kPa for G10D30H, which may owe to its less uniform porous structure compared to G10D20H as discussed previously. Containing 97 wt.% water, G10D20H is still impressive in its mechanical property; the presence of copious cross-linking points on every GO nanosheet and every PAMAM macromolecule (shown in Scheme 1), leads to the strong cross-linking interactions.

To examine the influence of GO on the viscoelastic parameters, rheological measurements were also undertaken on a series of hydrogels with various GO contents at a fixed concentration of PAMAM (20 mg mL⁻¹). In Fig. 7(C), the results show a monotonous rise in the storage moduli of the hydrogels with increasing GO content to 10 mg mL⁻¹, being 12, 44 and 284 kPa for G6D20H, G8D20H and G10D20H, respectively. A higher GO content (12 mg mL⁻¹) resulted in an unsuccessful preparation of hydrogel, which was observed during experiments due to the poor dispersion of GO nanosheets in the mixture (not shown). An increase in the GO content by 67% from G6D20H to G10D20H leads to an enhancement in the storage modulus by 23-fold. In contrast, an increase in the dendrimer content by 19-fold from G10D1H to G10D20H only induces an increase in the storage modulus by 16-fold. It is also noted, by comparing G10D10H or G10D5H with G6D20H, and G10D10H with G8D20H, that while the total content of GO and PAMAM in the hydrogel is lower, the hydrogel containing a higher content of GO shows a higher storage modulus. All of these results (Table 1) suggest that GO with a higher modulus than PAMAM contributes more significantly to the storage modulus of the nanocomposite hydrogel.¹⁴ Beside the content, the characteristics of GO, e.g., the lateral size and oxidation degree, will also influence the mechanical performance of the nanocomposite hydrogels. For

instance, a decrease in the lateral size of GO nanosheets leads to a lower aspect ratio, which makes GO less efficient in reinforcing polymers.⁵² It may also impact the dispersion of GO and the cross-linking density, again influencing the mechanical performance of the hydrogel. Similarly, a change to the oxidation degree of GO may affect the dispersion and cross-linking density as well as the mechanical properties of GO.

The highest storage modulus of 284 kPa reported herein for GO-PAMAM nanocomposite hydrogels is 247% of the highest modulus (115 kPa) for self-assembled GO-gelatin nanocomposite hydrogel,¹⁴ and 165% of the highest value (172 kPa) for the reduced GO-gelatin nanocomposite hydrogels⁵³ previously reported by our group. The storage moduli of these GO-PAMAM nanocomposite hydrogels are comparable to the values (10–400 kPa) of the GO-chitosan hydrogels reported by other researchers.¹⁵ Both GO and PAMAM dendrimer possess abundant functional groups which induce multiple strong cross-links on each GO nanosheet and each PAMAM macromolecule. Furthermore, the inherent high stiffness of GO also contributes to the high mechanical properties of the hydrogels effectively.



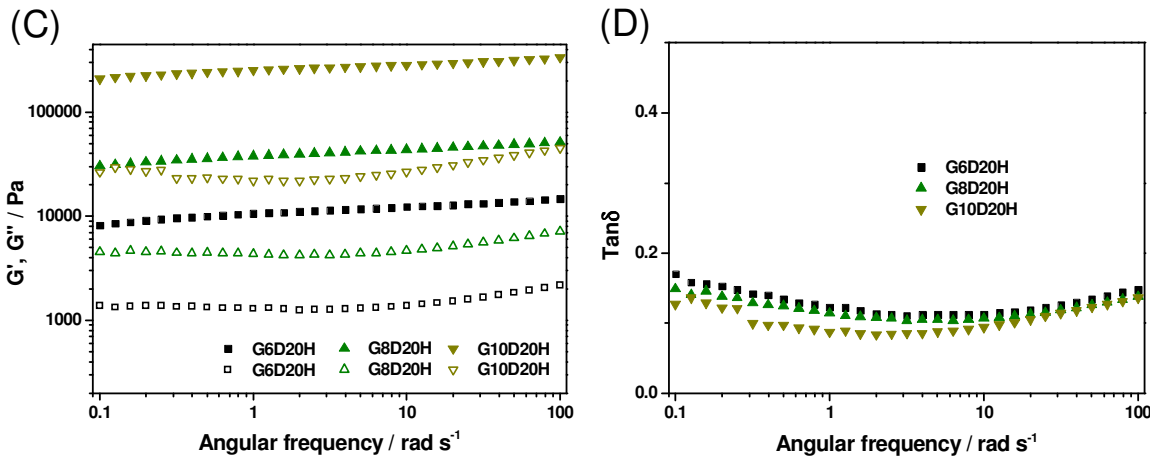


Figure 7. (A) G' (solid), G'' (hollow) and (B) $\tan\delta$ of GO-PAMAM hydrogels: G10D1H, G10D5H, G10D10H, G10D20H and G10D30H. (C) G' (solid), G'' (hollow) and (D) $\tan\delta$ of GO-PAMAM hydrogels: G6D20H, G8D20H and G10D20H.

The cross-linking density (N) and the number average molecular weight of the polymer chains between two neighbouring cross-links (\bar{M}_c) are important parameters of a hydrogel.⁵⁴ Assuming GO-PAMAM hydrogels are homogeneous Gaussian networks,^{14,53} these parameters can be calculated from the static shear modulus (G) data according to the rubber elasticity theory (Equation 1).⁵⁵

$$G = NkT = \frac{cRT}{\bar{M}_c} \left(1 - \frac{2\bar{M}_c}{M}\right) \quad (1)$$

Here, c is the polymer concentration in the hydrogel, R gas constant ($8.31 \text{ m}^3 \text{ Pa K}^{-1} \text{ mol}^{-1}$), T absolute temperature (298 K), M molecular weight of the polymer (9,534 for the PAMAM dendrimer) and k Boltzmann constant ($1.38065 \times 10^{-23} \text{ J K}^{-1}$). We previously deduced the relationship between G and G' (Equation 2)^{14,53}, based on the empirical correlation between static Young's modulus and dynamic Young's modulus⁵⁶ and the relationship between shear modulus and Young's modulus⁵⁷.

$$G = 0.629G' - \frac{1.586}{2(1+\nu)} \quad (2)$$

where ν is Poisson's ratio, for which 0.5 is used.⁵⁸ By inserting the known data into Equations 1 and 2, N and \overline{M}_c for the hydrogels are calculated and shown in Table 1.

Table 1. The rheological and cross-linking data of GO-PAMAM nanocomposite hydrogels

Sample	PAMAM (mg mL ⁻¹)	GO (mg mL ⁻¹)	Storage modulus, G' (kPa)	Cross-linking density, $N \times 10^{23}$ m ⁻³	Number average molecular weight, \overline{M}_c (g mol ⁻¹)
G10D1H	1	10	17	26.0	221
G10D5H	5	10	42	64.2	426
G10D10H	10	10	108	165.1	338
G10D20H	20	10	284	434.2	262
G10D30H	30	10	128	195.7	771
G8D20H	20	8	44	67.0	1299
G6D20H	20	6	12	18.8	2703

As shown in Table 1, N raises from 26.0×10^{23} m⁻³ for G10D1H to 434.2×10^{23} m⁻³ for G10D20H, having the same varying trend as that for G' . \overline{M}_c values are calculated to be 221, 426, 338 and 262 g mol⁻¹ for G10D1H, G10D5H, G10D10H and G10D20H, respectively. For those hydrogels with a fixed PAMAM content, N enhances from 18.8×10^{23} m⁻³ to 67.0×10^{23} m⁻³ and 434.2×10^{23} m⁻³ for G6D20H, G8D20H and G10D20H, respectively. Correspondingly, \overline{M}_c drops from 2,703 to 1,299 and 262 g mol⁻¹. The results illustrate a structure-property correlation that the hydrogel with a higher modulus possesses a higher cross-linking density, which is consistent with the literature.^{14,53}

4. CONCLUSIONS

GO-PAMAM dendrimer nanocomposite hydrogels with different concentrations of GO and PAMAM were synthesized through self-assembly in one step. The multiple electrostatic

interactions between GO sheets and PAMAM molecules, determined by FT-IR and Raman spectroscopy, provided the driving force for network formation.

These strong interactions rendered the nanocomposite hydrogels a high mechanical performance, with a storage modulus of up to 284 kPa at 10 mg mL⁻¹ GO and 20 mg mL⁻¹ PAMAM. At a fixed GO concentration (10 mg mL⁻¹), the storage modulus improved with PAMAM content first and then dropped under the studied range (up to 30 mg mL⁻¹). The critical concentration for PAMAM to construct a self-assembled GO-PAMAM nanocomposite hydrogel at this GO concentration was approximately 1.0 mg mL⁻¹. In contrast, the modulus of the self-assembled GO-PAMAM hydrogel increased with increasing GO content up to 10 mg mL⁻¹ at a fixed PAMAM content of 20 mg mL⁻¹, after which a hydrogel could not be formed. Compared to PAMAM, GO contributed more significantly to the storage modulus of the nanocomposite hydrogel. This kind of GO-PAMAM nanocomposite hydrogels could be explored for soft tissue engineering and drug delivery applications.

SUPPORTING INFORMATION

Digital images (Fig. S1 and Fig. S2) of GO-PAMAM nanocomposite hydrogels and their freshly cut hydrogel blocks before and after self-healing.

AUTHOR INFORMATION

Corresponding Author

* E-mail: binqiong.chen@sheffield.ac.uk; Fax: +44 (0)114 222 5943; Tel: +44 (0)114 222 5958.

Notes

The authors declare no competing financial interest.

ACKNOWLEDGMENTS

The authors thank the British Council and the Department of Business, Innovation and Skills for a Global Innovation Initiative grant (GII207).

REFERENCES

- (1) Hoffman, A. S. Hydrogels for biomedical applications. *Adv. Drug Delivery Rev.* **2002**, *54*, 3-12.
- (2) Drury, J. L.; Mooney, D. J. Hydrogels for tissue engineering: scaffold design variables and applications. *Biomaterials* **2003**, *24*, 4337-4351.
- (3) Suk, J. W.; Piner, R. D.; An, J.; Ruoff, R. S. Mechanical properties of monolayer graphene oxide. *ACS Nano* **2010**, *4*, 6557-6564.
- (4) Han, Y.; Lu, Y. Preparation and characterization of graphite oxide/polypyrrole composites. *Carbon* **2007**, *45*, 2394-2399.
- (5) Pu, W. D.; Zhang, L.; Huang, C. Z. Graphene oxide as a nano-platform for ATP detection based on aptamer chemistry. *Anal. Methods* **2012**, *4*, 1662-1666.
- (6) Chang, Y.; Yang, S.-T.; Liu, J.-H.; Dong, E.; Wang, Y.; Cao, A.; Liu, Y.; Wang, H. In vitro toxicity evaluation of graphene oxide on A549 cells. *Toxicol. Lett.* **2011**, *200*, 201-210.
- (7) Yang, K.; Gong, H.; Shi, X.; Wan, J.; Zhang, Y.; Liu, Z. In vivo biodistribution and toxicology of functionalized nano-graphene oxide in mice after oral and intraperitoneal administration. *Biomaterials* **2013**, *34*, 2787-2795.
- (8) Hou, C.; Zhang, Q.; Li, Y.; Wang, H. Graphene-polymer hydrogels with stimulus-sensitive volume changes. *Carbon* **2012**, *50*, 1959-1965.
- (9) Paul, A.; Hasan, A.; Kindi, H. A.; Gaharwar, A. K.; Rao, V. T.; Nikkhah, M.; Shin, S. R.; Krafft, D.; Dokmeci, M. R.; Shum-Tim, D. Injectable graphene oxide/hydrogel-based angiogenic gene delivery system for vasculogenesis and cardiac repair. *ACS Nano* **2014**, *8*, 8050-8062.
- (10) Bai, H.; Li, C.; Wang, X. L.; Shi, G. Q. A pH-sensitive graphene oxide composite hydrogel. *Chem. Commun.* **2010**, *46*, 2376-2378.
- (11) Xu, Y. X.; Wu, Q. O.; Sun, Y. Q.; Bai, H.; Shi, G. Q. Three-dimensional self-assembly of graphene oxide and DNA into multifunctional hydrogels. *ACS Nano* **2010**, *4*, 7358-7362.
- (12) Bai, H.; Li, C.; Wang, X.; Shi, G. On the gelation of graphene oxide. *J. Phys. Chem. C* **2011**, *115*, 5545-5551.
- (13) Adhikari, B.; Biswas, A.; Banerjee, A. Graphene oxide-based hydrogels to make metal nanoparticle-containing reduced graphene oxide-based functional hybrid hydrogels. *ACS Appl. Mater. Interf.* **2012**, *4*, 5472-82.
- (14) Piao, Y.; Chen, B. Self-assembled graphene oxide-gelatin nanocomposite hydrogels: characterization, formation mechanisms, and pH-sensitive drug release behavior. *J. Polym. Sci. B* **2015**, *53*, 356-367.

- (15) Chen, Y.; Chen, L.; Bai, H.; Li, L. Graphene oxide-chitosan composite hydrogels as broad-spectrum adsorbents for water purification. *J. Mater. Chem. A* **2013**, *1*, 1992-2001.
- (16) Guo, H.; Jiao, T.; Zhang, Q.; Guo, W.; Peng, Q.; Yan, X. Preparation of graphene oxide-based hydrogels as efficient dye adsorbents for wastewater treatment. *Nanoscale Res. Lett.* **2015**, *10*, 1-10.
- (17) Han, D.; Yan, L. Supramolecular hydrogel of chitosan in the presence of graphene oxide nanosheets as 2D cross-linkers. *ACS Sustain. Chem. Eng.* **2013**, *2*, 296-300.
- (18) Tomalia, D. A. Birth of a new macromolecular architecture: dendrimers as quantized building blocks for nanoscale synthetic polymer chemistry. *Prog. Polym. Sci.* **2005**, *30*, 294-324.
- (19) Choi, S. K.; Thomas, T. P.; Li, M.-H.; Desai, A.; Kotlyar, A.; Baker, J. R. Photochemical release of methotrexate from folate receptor-targeting PAMAM dendrimer nanoconjugate. *Photochem. Photobiol. Sci.* **2012**, *11*, 653-660.
- (20) Zhong, S.; Yung, L. Y. L. Enhanced biological stability of collagen with incorporation of PAMAM dendrimer. *J. Biomed. Mater. Res. A* **2009**, *91*, 114-122.
- (21) Desai, P. N.; Yuan, Q.; Yang, H. Synthesis and characterization of photocurable polyamidoamine dendrimer hydrogels as a versatile platform for tissue engineering and drug delivery. *Biomacromolecules* **2010**, *11*, 666-673.
- (22) Yang, H.; Tyagi, P.; Kadam, R. S.; Holden, C. A.; Kompella, U. B. Hybrid dendrimer hydrogel/PLGA nanoparticle platform sustains drug delivery for one week and antiglaucoma effects for four days following one-time topical administration. *ACS Nano* **2012**, *6*, 7595-7606.
- (23) Wang, Q.; Mynar, J. L.; Yoshida, M.; Lee, E.; Lee, M.; Okuro, K.; Kinbara, K.; Aida, T. High-water-content mouldable hydrogels by mixing clay and a dendritic molecular binder. *Nature* **2010**, *463*, 339-343.
- (24) Wu, T.; Wang, X.; Qiu, H.; Gao, J.; Wang, W.; Liu, Y. Graphene oxide reduced and modified by soft nanoparticles and its catalysis of the Knoevenagel condensation. *J. Mater. Chem.* **2012**, *22*, 4772-4779.
- (25) Kim, J. M.; Kim, J.; Kim, J. Covalent decoration of graphene oxide with dendrimer-encapsulated nanoparticles for universal attachment of multiple nanoparticles on chemically converted graphene. *Chem. Commun.* **2012**, *48*, 9233-9235.
- (26) Luo, Z.; Yuwen, L.; Han, Y.; Tian, J.; Zhu, X.; Weng, L.; Wang, L. Reduced graphene oxide/PAMAM-silver nanoparticles nanocomposite modified electrode for direct electrochemistry of glucose oxidase and glucose sensing. *Biosen. Bioelectron.* **2012**, *36*, 179-185.
- (27) Yuan, Y.; Zhang, G.; Li, Y.; Zhang, G.; Zhang, F.; Fan, X. Poly(amidoamine) modified graphene oxide as an efficient adsorbent for heavy metal ions. *Polym. Chem.* **2013**, *4*, 2164-2167.
- (28) Zhang, F.; Wang, B.; He, S.; Man, R. Preparation of graphene-oxide/polyamidoamine dendrimers and their adsorption properties toward some heavy metal ions. *J. Chem. Eng. Data* **2014**, *59*, 1719-1726.

- (29) Yu, Y.; De Andrade, L. C. X.; Fang, L.; Ma, J.; Zhang, W.; Tang, Y. Graphene oxide and hyperbranched polymer-toughened hydrogels with improved absorption properties and durability. *J. Mater. Sci.* **2015**, *50*, 3457-3466.
- (30) Mintzer, M. A.; Grinstaff, M. W. Biomedical applications of dendrimers: a tutorial. *Chem. Soc. Rev.* **2011**, *40*, 173-190.
- (31) Tomalia, D. A.; Baker, H.; Dewald, J.; Hall, M.; Kallos, G.; Martin, S.; Roeck, J.; Ryder, J.; Smith, P. A new class of polymer: starburst-dendritic macromolecules. *Polym. J.* **1985**, *17*, 117-132.
- (32) Tomalia, D. A.; Baker, H.; Dewald, J.; Hall, M.; Kallos, G.; Martin, S.; Roeck, J.; Ryder, J.; Smith, P. Dendritic macromolecules: synthesis of starburst dendrimers. *Macromolecules* **1986**, *19*, 2466-2468.
- (33) Hummers, W. S.; Offeman, R. E. Preparation of graphitic oxide. *J. Am. Chem. Soc.* **1958**, *80*, 1339-1339.
- (34) Marcano, D. C.; Kosynkin, D. V.; Berlin, J. M.; Sinitskii, A.; Sun, Z. Z.; Slesarev, A.; Alemany, L. B.; Lu, W.; Tour, J. M. Improved synthesis of graphene oxide. *ACS Nano* **2010**, *4*, 4806-4814.
- (35) Choi, J. S.; Nam, K.; Park, J.-Y.; Kim, J.-B.; Lee, J.-K.; Park, J.-S. Enhanced transfection efficiency of PAMAM dendrimer by surface modification with L-arginine. *J. Control. Release* **2004**, *99*, 445-456.
- (36) Shi, X.; Bánya, I.; Islam, M. T.; Lesniak, W.; Davis, D. Z.; Baker, J. R.; Balogh, L. P. Generational, skeletal and substitutional diversities in generation one poly(amidoamine) dendrimers. *Polymer* **2005**, *46*, 3022-3034.
- (37) Kim, Y.; Klutz, A. M.; Jacobson, K. A. Systematic investigation of polyamidoamine dendrimers surface-modified with poly(ethylene glycol) for drug delivery applications: synthesis, characterization, and evaluation of cytotoxicity. *Bioconjugate Chem.* **2008**, *19*, 1660-1672.
- (38) Shi, X.; Lesniak, W.; Islam, M. T.; Muñiz, M. C.; Balogh, L. P.; Baker, J. R. Comprehensive characterization of surface-functionalized poly(amidoamine) dendrimers with acetamide, hydroxyl, and carboxyl groups. *Colloid. Surf. A* **2006**, *272*, 139-150.
- (39) Szabó, T.; Tombácz, E.; Illés, E.; Dékány, I. Enhanced acidity and pH-dependent surface charge characterization of successively oxidized graphite oxides. *Carbon* **2006**, *44*, 537-545.
- (40) Petit, C.; Seredych, M.; Bandosz, T. J. Revisiting the chemistry of graphite oxides and its effect on ammonia adsorption. *J. Mater. Chem.* **2009**, *19*, 9176-9185.
- (41) Kataoka, T.; Kidowaki, M.; Zhao, C.; Minamikawa, H.; Shimizu, T.; Ito, K. Local and network structure of thermoreversible polyrotaxane hydrogels based on poly(ethylene glycol) and methylated β -cyclodextrins. *J. Phys. Chem. B* **2006**, *110*, 24377-24383.
- (42) Zhang, Y.-P.; Xu, J.-J.; Sun, Z.-H.; Li, C.-Z.; Pan, C.-X. Preparation of graphene and TiO₂ layer by layer composite with highly photocatalytic efficiency. *Prog. Nat. Sci.* **2011**, *21*, 467-471.

- (43) Gautam, P.; Gupta, A. K.; Sharma, A.; Gautam, T. Synthesis and analytical characterization of ester and amine terminated PAMAM dendrimers. *Global J. Med. Res.* **2013**, *13*, 7-15.
- (44) Bourlinos, A. B.; Gournis, D.; Petridis, D.; Szabó, T.; Szeri, A.; Dékány, I. Graphite oxide: chemical reduction to graphite and surface modification with primary aliphatic amines and amino acids. *Langmuir* **2003**, *19*, 6050-6055.
- (45) Park, S.; Dikin, D. A.; Nguyen, S. T.; Ruoff, R. S. Graphene oxide sheets chemically cross-linked by polyallylamine. *J. Phys. Chem. C* **2009**, *113*, 15801-15804.
- (46) Tuinstra, F.; Koenig, J. L. Raman spectrum of graphite. *J. Chem. Phys.* **1970**, *53*, 1126-1130.
- (47) Ferrari, A. C. Raman spectroscopy of graphene and graphite: disorder, electron-phonon coupling, doping and nonadiabatic effects. *Solid State Commun.* **2007**, *143*, 47-57.
- (48) Li, J.; Liu, C.-Y.; Liu, Y. Au/graphene hydrogel: synthesis, characterization and its use for catalytic reduction of 4-nitrophenol. *J. Mater. Chem.* **2012**, *22*, 8426-8430.
- (49) Liang, J.; Huang, Y.; Zhang, L.; Wang, Y.; Ma, Y.; Guo, T.; Chen, Y. Molecular-level dispersion of graphene into poly(vinyl alcohol) and effective reinforcement of their nanocomposites. *Adv. Funct. Mater.* **2009**, *19*, 2297-2302.
- (50) Hager, M. D.; Greil, P.; Leyens, C.; van der Zwaag, S.; Schubert, U. S. Self-healing materials. *Adv. Mater.* **2010**, *22*, 5424-5430.
- (51) Juby, K.; Dwivedi, C.; Kumar, M.; Kota, S.; Misra, H.; Bajaj, P. Silver nanoparticle-loaded PVA/gum acacia hydrogel: synthesis, characterization and antibacterial study. *Carbohydr. Polym.* **2012**, *89*, 906-913.
- (52) Sheng, N.; Boyce, M. C.; Parks, D. M.; Rutledge, G.; Abes, J.; Cohen, R. Multiscale micromechanical modeling of polymer/clay nanocomposites and the effective clay particle. *Polymer* **2004**, *45*, 487-506.
- (53) Piao, Y.; Chen, B. One-pot synthesis and characterization of reduced graphene oxide-gelatin nanocomposite hydrogels. *RSC Adv.* **2016**, *6*, 6171-6181.
- (54) Lee, K. Y.; Rowley, J. A.; Eiselt, P.; Moy, E. M.; Bouhadir, K. H.; Mooney, D. J. Controlling mechanical and swelling properties of alginate hydrogels independently by cross-linker type and cross-linking density. *Macromolecules* **2000**, *33*, 4291-4294.
- (55) Treloar, L. R. G. *The physics of rubber elasticity*. Oxford University Press: USA, 1975; p 1-2, 160-170.
- (56) Sabbagh, J.; Vreven, J.; Leloup, G. Dynamic and static moduli of elasticity of resin-based materials. *Dent. Mater.* **2002**, *18*, 64-71.
- (57) Meyvis, T. K. L.; Stubbe, B. G.; Van Steenbergen, M. J.; Hennink, W. E.; De Smedt, S. C.; Demeester, J. A comparison between the use of dynamic mechanical analysis and oscillatory shear rheometry for the characterisation of hydrogels. *Int. J. Pharm.* **2002**, *244*, 163-168.
- (58) Macosko, C. *Rheology: principles, measurements, and applications*. VCH: New York, 1994, p 37-45.